How to Cite: Abdulsattar, M.A. (2024). Effect of Acetylene Properties on its Gas Sensing by NiO Doped ZnO Clusters: A Transition State Theory Model. *Eurasian Journal of Chemistry, 29, 4(116), 35–43.* https://doi.org/10.31489/2959-0663/4-24-8

Article

Received: 29 July 2024 | Revised: 18 October 2024 |
Accepted: 31 October 2024 | Published online: 23 November 2024

UDC 544.4+544.18

https://doi.org/10.31489/2959-0663/4-24-8

Mudar A. Abdulsattar*

Ministry of Science and Technology, Baghdad, Iraq
*(*Author`s e-mail: mudarahmed3@yahoo.com)*

Effect of Acetylene Properties on its Gas Sensing by NiO Doped ZnO Clusters: A Transition State Theory Model

The sensitivity of nickel oxide doped zinc oxide to industrial gas acetylene was calculated and compared to available experimental data. The adsorption of C_2H_2 on the NiO-doped ZnO surface and the activation transition states formed afterward were studied computationally. B3LYP version of density functional theory with 6-311G** basis set, including dispersion correction (GD3BJ) was performed for the calculations with the help of Gaussian 09 software. Thermodynamic quantities of the reaction of C_2H_2 with NiO-doped ZnO surfaces, such as Gibbs free energy, enthalpy, and entropy, were used to interpret the reaction at the temperature range 25–325 °C. Response and response time variation with different NiO doping percentages were calculated. The calculations took into account the combustion of acetylene as it approached its autoignition temperature, which was not considered in previous works. The results show that the optimum response operating temperature of the C_2H_2 gas sensor is below the autoignition temperature of acetylene at 300 °C. A good agreement of theoretical response and response time with variation of temperature and acetylene concentration was obtained with the experiment. This study was the first to take into account the autoignition of C_2H_2 in gas sensor calculations and noted that gases can be easily distinguished by their autoignition temperature.

Keywords: NiO-doping, ZnO cluster, acetylene gas sensor, Density Functional Theory, transition state.

Introduction

ZnO is in the hexagonal wurtzite structure [1], while NiO is in the NaCl cubic structure at ambient temperature [2]. When ZnO is doped with NiO, the hexagonal structure is transformed into a cubic NaCl structure as the NiO doping concentration increases [3]. ZnO in the NaCl structure occurs at high pressure [4]. On the other hand, the NiO in the hexagonal structure is also formed [5]. ZnO is an n-type semiconductor due to oxygen vacancies [6]. NiO is a p-type semiconductor since Ni can have higher oxides such as Ni_2O_3 (black nickel oxide) [7]. The doping of ZnO with NiO can form a *p-n* junction. ZnO is a very practical choice for gas sensors. ZnO is used to detect many gases, such as acetone [8], acetaldehyde [9], NO_2 [10], etc. NiO as an oxide is also utilized as a gas sensor for different gases such as H_2S [11], acetone [12], H_2 [13], etc. Small ZnO clusters that reflect the wurtzite structure are called wurtzoids [14, 15]. These clusters simplify gas sensor calculations within existing computing power while preserving the similarity of the electronic structure with particles of larger size. The gas-sensing process happens on the surface of the sensor. Since oxygen layers are inevitable during surface preparation under atmospheric conditions, Ni atoms on the surface are oxidized by the oxygen in the air or by oxygen already present in the ZnO.

Acetylene is an unsaturated hydrocarbon with the formula C_2H_2, widely used in industry [16]. Acetylene has a number of properties that differ from many other gases. C_2H_2 is a sublimating gas at about –84 °C. It also has an autoignition temperature of 300 °C. Autoignition temperature is the temperature at which a material will spontaneously ignite in a normal atmosphere without the need for an external ignition source. This temperature puts limits on the highest temperature at which the gas can be detected, since it quickly burns out after reaching this temperature [17, 18]. The intrinsic properties of the detected gas are continuously ignored when calculating gas detection in a sensor. In the present work the properties of acetylene will play an important role in the detection of this gas, as we shall see later.

Transition state theory is one of the most used theories to simulate reactions that include gas sensors [19]. The parameters of this theory can be calculated using density functional theory (DFT). These parameters include thermodynamic quantities such as Gibbs free energy of activation, enthalpy, and entropy. These parameters usually depend on temperature.

The present work uses a NiO-doped ZnO cluster as a gas sensor to detect acetylene gas. The analysis is carried out theoretically using transition state theory and compared with available experimental data. Gibbs

free energy of transition or activation is calculated as a function of temperature. The calculated Gibbs energy of transition is transformed to the values of the experimental NiO-doped ZnO ratio using the modified Evans–Polanyi principle. The change in the density of acetylene gas as acetylene approaches its autoignition temperature is considered. Results show good agreement of theoretically calculated sensor response and response time with available experimental data. The novelty and motivation of the present work are derived from the fact that acetylene autoignition has never been considered in previous studies.

Computational Details

Gaussian 09 computational chemistry software was used in the present calculations [20]. B3LYP version of density functional theory with 6-311G** basis set, including dispersion correction (GD3BJ), showed satisfactory accuracy and execution time [21].

ZnO small clusters similar to the hexagonal wurtzite bulk structure are called wurtzoids [15, 22]. These clusters have been used frequently to replace the time-consuming periodic representation of bulk ZnO, including doping with different elements [14, 23]. Figure 1 shows the adsorption of C_2H_2 on pristine and NiO-doped ZnO clusters ($Zn_{13}O_{13}$ and $NiZn_{12}O_{13}$).

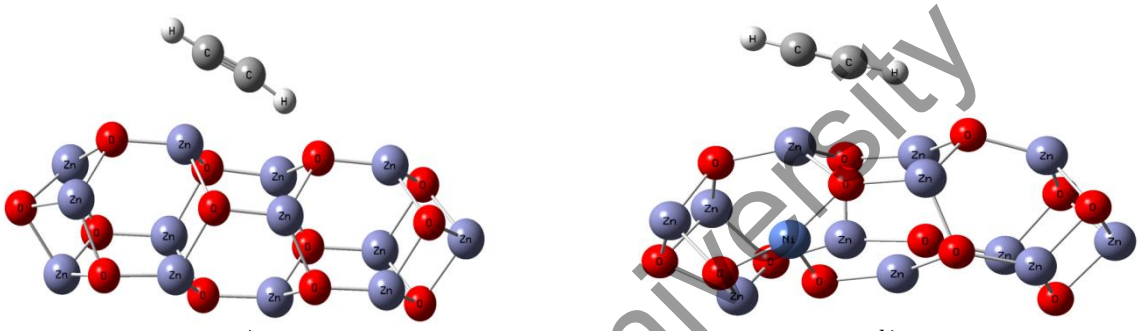

a) *b*)

Figure 1. *a* — The adsorption of C_2H_2 on optimized pristine ZnO clusters ($Zn_{13}O_{13}$) designed as $[Zn_{13}O_{13} – C_2H_2]^a$; *b* — optimized $NiZn_{12}O_{13}$ with adsorbed C_2H_2 molecule designed as $[NiZn_{12}O_{13} – C_2H_2]^a$

The interaction between the cluster and acetylene diminishes as the number of neighbors increases. Typically, a fourth neighbor interaction cutoff is used so that results are highly correct with negligible remaining interactions [24]. Adsorption is characterized by the attraction of hydrogen atoms in C_2H_2 to oxygen atoms on pristine or doped ZnO. On the other hand, carbon atoms in C_2H_2 are attracted to Zn or Ni atoms. This van der Waals attraction is due to the positive charges on H, Zn, and Ni atoms and negative charges on C and O atoms. It can be noted that the Ni atom is connected to oxygen atoms (O–Ni–O angle), forming nearly 90- or 180-degree angles with them, which reflects the NaCl structure characterization of NiO.

After adsorption, a transition state is formed before the interaction of C_2H_2 with pristine and NiO-doped ZnO clusters. The transition state is defined as the state of the highest potential energy along the reaction path. The transition states developed from the adsorption states of Figure 1 are shown in Figure 2. The (TS) option of Gaussian 09 program using the Berny algorithm is adopted.

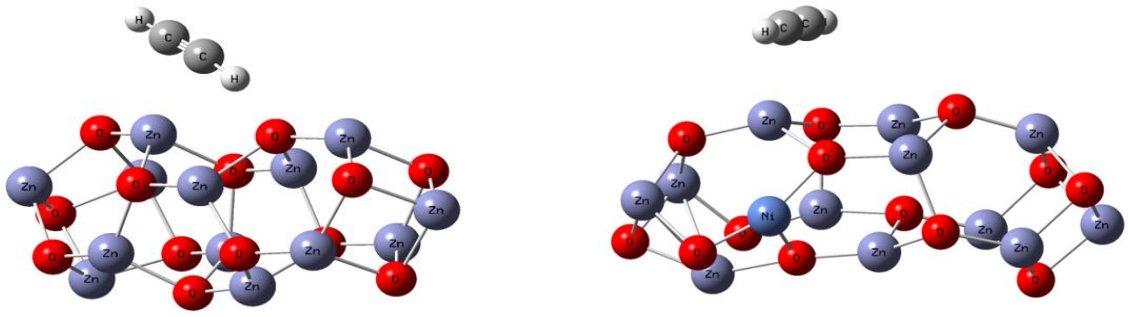

a) *b*)

Figure 2. *a* — The optimized transition state of adsorbed C_2H_2 on pristine ZnO ($[Zn_{13}O_{13} – C_2H_2]^‡$); *b* — The optimized transition state of $NiZn_{12}O_{13}$ with adsorbed C_2H_2 molecule $[NiZn_{12}O_{13} – C_2H_2]^‡$

As can be seen from Fig. 2, the C_2H_2 molecule encounters a rotation from the adsorption state of Fig. 1. This rotation is more evident in the NiO-doped ZnO cluster in Fig. 2*b*.

The rate of a chemical reaction is influenced by several factors such as temperature, pressure, and concentration of the reacting materials. Many theories have been proposed to handle and calculate such rates, including the Arrhenius equation, collision theory, and transition state theory and their variations. At constant pressure, the general equation describing the reaction rate for the present reaction of ZnO with acetylene can be given as follows [25]:

$$\frac{d[\mathrm{ZnO}]}{dt} = -[\mathrm{ZnO}]^u [\mathrm{C_2H_2}]_e^v k(T), \tag{1}$$

$$k(T) = AT^m \exp^{\left(\frac{-\Delta G^{\ddagger}}{k_B T}\right)}. \tag{2}$$

In the above two equations, [ZnO] and [C_2H_2] are the zinc oxide and acetylene concentrations, respectively. The exponents *u* and *v* in the concentrations are usually equal to 1 or ½. The subscript *e* in the acetylene concentration represents the effective concentration of acetylene due to autoignition as acetylene approaches its autoignition temperature. *k*(*T*) represents the effect of temperature on the reaction rate. The temperature dependence *k*(*T*) reflects the type of gas and sensor, as well as the ability of the gas to diffuse into the sensor surface and reach the inner layers. The value of *m* for the temperature exponent in Eq. (2) is higher for gases that can diffuse deep in the sensor's layers. $\Delta G^{\ddagger}$ is the Gibbs energy of transition, while k_B is the Boltzmann constant. The effect of material properties such as morphology, surface area, crystallinity, and structure is inhibited in the pre-exponential parameter (*A*) in the *k*(*T*) equation (Eq. (2)).

Evaluating the Gibbs transition energy for NiO-doped ZnO can sometimes be difficult since the exact doping percentage may involve many atoms, requiring a long computational time. However, a solution can be proposed using the modified Evans–Polanyi principle as follows [25]:

$$\Delta G^{\ddagger} = \Delta G_0^{\ddagger} + \beta \Delta G_1^{\ddagger}, \tag{3}$$

In the above equation, $\Delta G_0^{\ddagger}$ and $\Delta G_1^{\ddagger}$ are known Gibbs energy of transition of two structures that are near the required $\Delta G^{\ddagger}$ value using the interpolation parameter β. The values of $\Delta G_0{}^{\ddagger}$ and $\Delta G_1{}^{\ddagger}$ are that of pristine and NiO-doped ZnO in Fig. 2*a* and Fig. 2*b* respectively. Their values are 0.1487 and 0.1377 eV (at standard 25 °C and 1 bar conditions) respectively. The interpolation parameter β can be found using simple linear interpolation formulas. The original Evans–Polanyi principle concerns the interpolation of enthalpy $\Delta H^{\ddagger}$. The addition of the activation entropy ($S^{\ddagger}$) transforms the relation to a Gibbs energy relation:

$$\Delta G^{\ddagger} = \Delta H^{\ddagger} - T\Delta S^{\ddagger}. \tag{4}$$

As mentioned in the description of Eq. (1), the effective concentration of acetylene is used due to the ignition of acetylene as its autoignition temperature of 300 °C approaches. A logistic function is used to describe the concentration of acetylene as it approaches the autoignition temperature [18]:

$$f(T) = \frac{1}{1 + e^{k_s(T - T_0)}}, \tag{5}$$

where k_s is the steepness of the decrease in acetylene concentration, T_0 is the temperature at which acetylene reaches half of its original concentration as it approaches autoignition temperature.

Eq. (5) is the critical equation that will shape the gas response curves that follow Eq. (1) for the reaction rate.

The detection of the acetylene gas is performed as a consequence of monitoring sensor resistance changes due to the reaction of acetylene with the sensing material. The sensor's resistance in the air is denoted R_a, while the resistance in the presence of a gas is denoted R_g. The ratio R_a/R_g is called the sensor's response. This ratio is proportional to the reaction rate of Eq. (1), as in the following equation:

$$\mathrm{Response(theoretical)} = 1 + C\left|\frac{d[\mathrm{ZnO}]}{dt}\right| \tag{6}$$

The value (1) is added in Eq. (6) because the response is 1 in the absence of gas ($R_a/R_g = 1$). *C* is the correlation factor linking the resistivity to the reaction rate.

An important quantity that measures the fast response of the gas sensor is the response time (t_{res}). This quantity can be obtained by integrating Eq. (1) concerning time (*t*) with the exponent ($u = 1$) in Eq. (1). The response time, which corresponds to the time needed for the resistivity to reach 90 % of its final resistance, is determined by the following formula [25]:

$$t_{res(90\ \%)} = \frac{\ln(10)}{[C_2H_2]_e^{v}\, AT^{m}\, \exp\left(\frac{-\Delta G^{\ddagger}}{k_B T}\right)} \tag{7}$$

Results and Discussion

Fig. 3 shows the variation of Gibbs free energy in the transition of pure and NiO-doped ZnO with temperature.

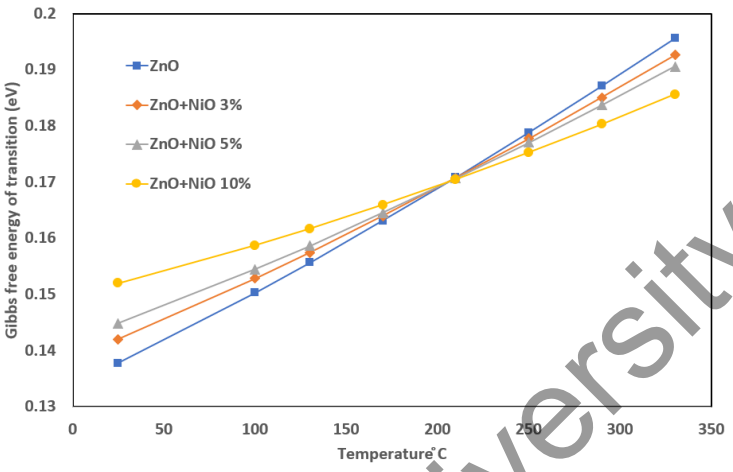

Figure 3. The Gibbs free energy of transition of the optimized transition state of adsorbed C_2H_2 on the four cases of pristine and 3, 5, 10 % NiO-doped ZnO as a function of temperature

As can be seen in Fig. 3, the Gibbs free energy of transition of pure and NiO doped ZnO are close and intersect at a temperature of 210 °C. This temperature has the same highest response and lowest response time, as seen in the corresponding figures.

Fig. 4 shows the change in theoretical response (R_a/R_g) for different NiO concentrations (3, 5, 10 % molar ratio) with temperature compared with experimental results [26] for 200 ppm C_2H_2. The autoignition temperature of C_2H_2 is indicated.

As can be seen in Fig. 4, using the present theory, good agreement was obtained between the theoretical and experimental results. The maximum response is at 210 °C for all theoretical calculations in good agreement with the two NiO doping percentages 3 and 5 %, while the experimental 10 % NiO percentage deviates at 160 °C. Most available experimental data from other experiments agree with present theoretical results. As an example, the maximum response of C_2H_2 is at 206, 255, 200, 250, and 285 °C for the references [27–31], respectively that are all below the autoignition temperature at 300 °C in agreement with present results. The present calculations provide a unique method to distinguish gases. As an example, the H_2 autoignition temperature is at 536 °C that is far from that of acetylene and its maximum response can be distinguished easily.

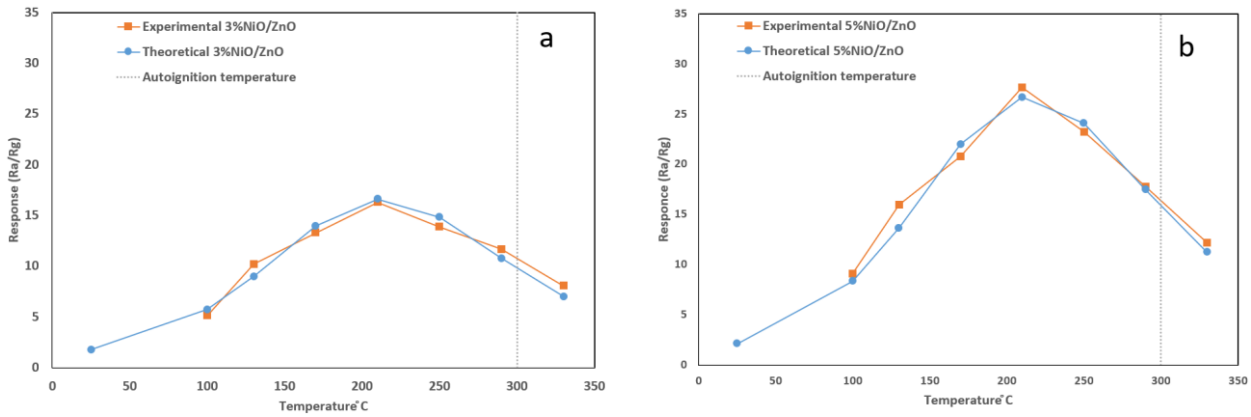

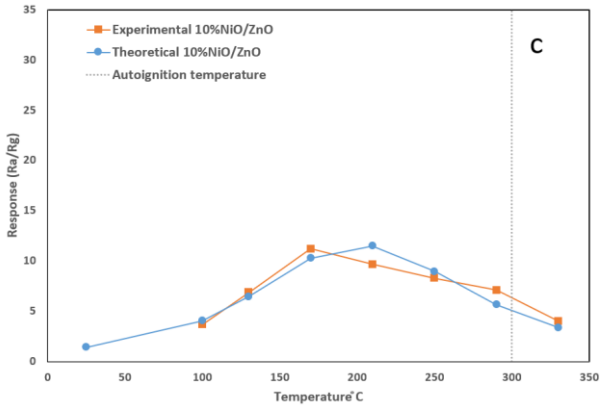

Figure 4. Change in theoretical response (R_a/R_g) for different NiO concentrations (3, 5, 10 % molar ratio) with temperature compared with experimental results [26] for 200 ppm C_2H_2. The autoignition temperature of C_2H_2 is indicated

Fig. 5 shows the change in theoretical response (R_a/R_g) for different NiO concentrations (3, 5, 10 % molar ratio) with C_2H_2 concentration at 210 °C temperature compared with experimental results [26]. Good agreement can be seen between the experimental and theoretical results. The highest response is for 5 % NiO doping, as shown in Fig. 4.

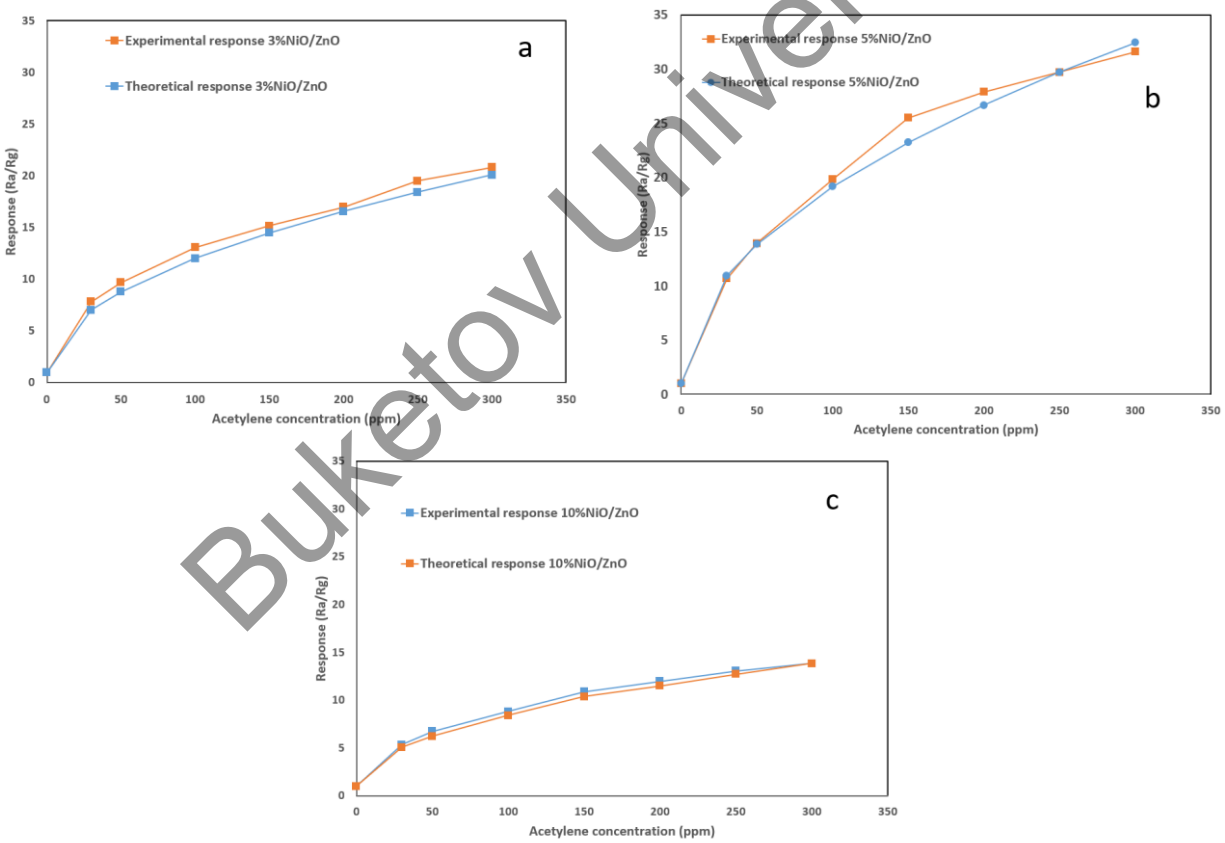

Figure 5. Change in theoretical response (R_a/R_g) for different NiO concentrations (3, 5, 10 % molar ratio) with C_2H_2 concentration at 210 °C compared to experimental results [26]

Table shows the parameters used in the simulation for the three different NiO doping percentages of ZnO.

Table

Parameters used to simulate the C_2H_2 gas sensing reaction model for different NiO-doped ZnO $\Delta G^{\ddagger}$ values are at 25℃ and normal pressure

No.	Reaction	$\Delta G^{\ddagger}$ (eV)	A	m	v	k_s (K^{-1})	T_0 (°C)	C (s)
1	[3 %NiO/ZnO – C_2H_2]^a ↓ [3 % NiO/ZnO – C_2H_2]‡	0.142	$3.5 \cdot 10^{-11}$ $s^{-1} \cdot K^{-5}$	5	½	0.025	200	165
2	[5 % NiO/ZnO – C_2H_2]^a ↓ [5 % NiO/ZnO – C_2H_2]‡	0.145	$5 \cdot 10^{-11}$ $s^{-1} \cdot K^{-5}$	5	½	0.025	200	190
3	[10 % NiO/ZnO – C_2H_2]^a ↓ [10 % NiO/ZnO – C_2H_2]‡	0.152	$2.9 \cdot 10^{-11}$ $s^{-1} \cdot K^{-5}$	5	½	0.03	195	150

As can be seen in Table, the value of the Gibbs free energy of the transition rises as the doping percentage of NiO increases. However, at temperatures above 210 °C, the opposite trend was observed, as shown in Fig. 3. Parameter A has the highest value for the 5 % NiO doping percentage, which is also typical for the parameter C. This explains the highest sensitivity at 5 % NiO doping percentage. As the doping percentage rises, the reaction rate and sensitivity increase because of the destruction of the lattice periodicity. A further rise in the doping percentage (more than 5 %) will not lead to an increase in two parameters, *A* and *C*, since the lattice is already developing a new NiO cubic phase at the spots of higher concentration of NiO.

The value of the temperature exponent (m = 5) is the same for all doping percentages. This exponent reflects the reactivity and diffusivity of the C_2H_2 gas. In the original transition state theory, which did not take diffusivity into account, the value of *m* was equal to 1. The exponent *v*'s value is ½, which was also typical in many doping cases [32].

The remaining parameters, k_s and T_0, have the same value for 3 % and 5 % NiO doping and slightly change for the 10 % NiO doping. These two parameters represent the decay in the concentration of C_2H_2 gas as it reaches its autoignition temperature. The almost equal values of k_s and T_0 show that the autoignition temperature depends only slightly on the type of sensitive material.

Fig. 6 shows the response time of the three different doping percentages of NiO as described by Eq. (7) compared to the experiment. Fig. 6 shows the reverse to Fig. 4 trend in response time. The response time is at its lowest value when the response is at its highest value. Good agreement is obtained between theory and experiment.

Fig. 7 explains the effect of doping ZnO by NiO. The energy gap is defined as the difference between the Lowest Unoccupied Molecular Orbital (LUMO) and the Highest Occupied Molecular Orbital (HOMO) energies. The experimental energy gap of ZnO is 3.3 eV [33]. This value is close to the present calculated value of 3.117 eV as in Fig. 7. As ZnO is doped with NiO (Fig. 1*b*), the energy gap decreases to 2.412 eV due to the entrance of NiO energy levels into the energy gap of ZnO and the destruction of the original hexagonal structure. The gap value for NiO is around 3 eV [34]. As the NiO doping increases, the energy gap increases to 3 eV when the cubic NiO structure becomes the dominant constituent.

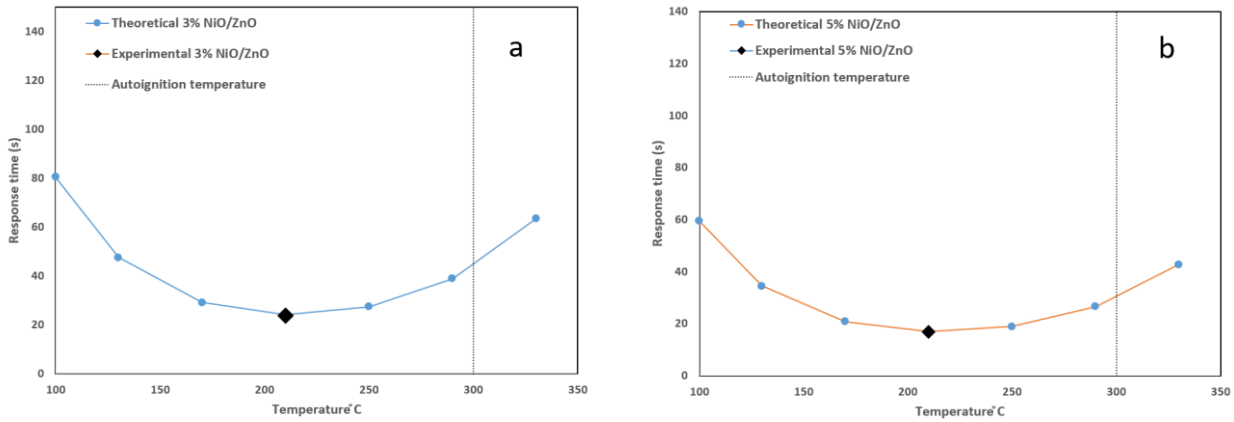

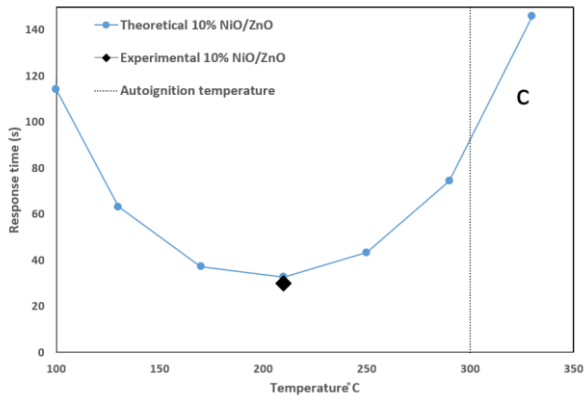

Figure 6. Experimental [26] and theoretical response time for the three cases of 3, 5, and 10 % NiO doped ZnO sensor as a function of temperature. The autoignition temperature of C_2H_2 is shown

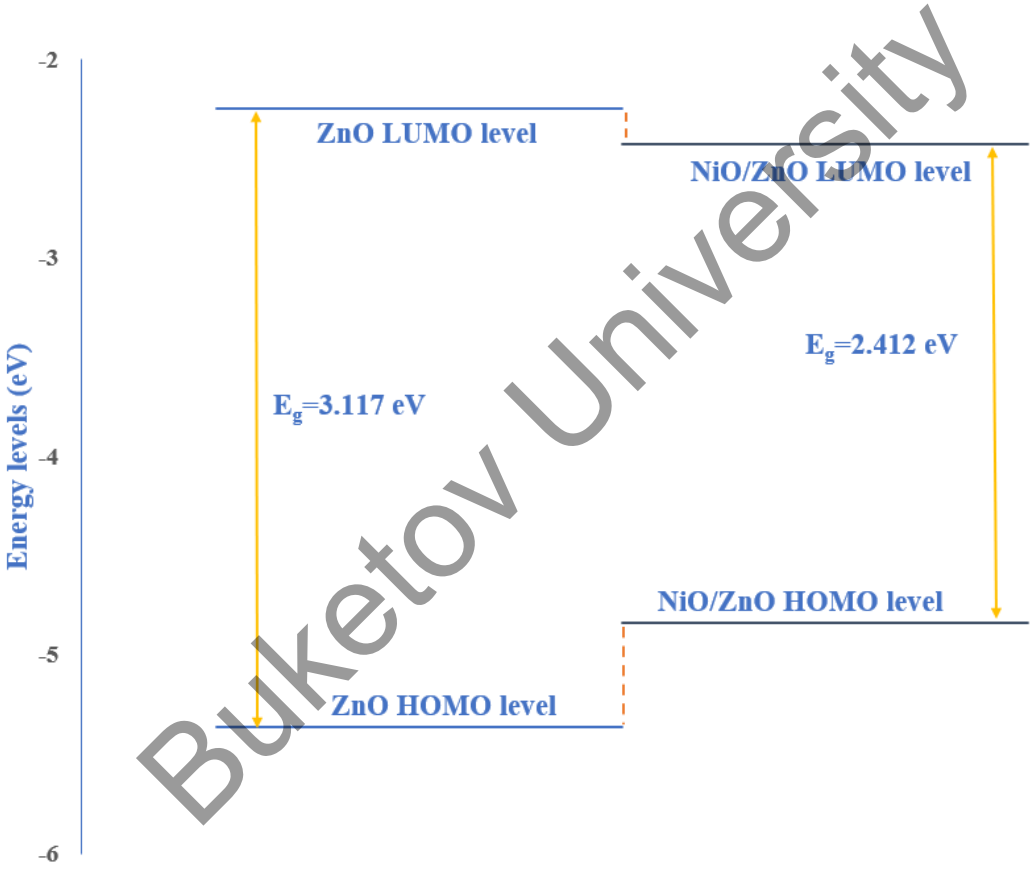

Figure 7. Calculated HOMO and LUMO energy levels for ZnO and NiO/ZnO.
The NiO/ZnO corresponds to the optimized $NiZn_{12}O_{13}$ in Fig. 1*b*

Conclusions

NiO-doped ZnO gas sensor cluster was studied theoretically to detect C_2H_2 gas as a function of temperature and compared with available experimental data. The transition state theory with a modified Evans–Polanyi principle was used to estimate the Gibbs free transition energy for three different doping cases. The theoretical investigation was carried out using mainly two equations, namely Eq. (1) and Eq. (5). As the temperature increases, the C_2H_2 gas burns using the oxygen available in the air, and the concentration of the C_2H_2 gas decreases as described by Eq. (5). At the same time, C_2H_2 gas reacts with the sensing material NiO doped ZnO as described by Eq. (1). The result shows a maximum of sensing temperature, which is below the

autoignition temperature of acetylene of 300 °C. The above described model is in good agreement with the experiment presented in Figs (4–6) for the three different NiO doping concentrations. Figs (4–6) show the theoretical and experimental response results taking into account temperature, concentration, and response time. The motivation for the present study is that the autoignition of C_2H_2 has never been taken into account in gas sensor calculations, and gases can be easily distinguished by their autoignition temperature.

*Author Information**

**The authors' names are presented in the following order: First Name, Middle Name and Last Name*

Mudar Ahmed Abdulsattar — Chief Scientific Researcher, Head of Solid-State Department, Ministry of Science and Technology, Baghdad, Iraq, *e-mail*: mudarahmed3@yahoo.com; https://orcid.org/0000-0001-8234-6686

Conflicts of Interest

The authors declare no conflict of interest.

References

1 Karmakar, A., Chakraborty, T., Chakravarty, S., Nath, M., Chakraborty, S., Mitra, S., Sarkar, S., Mandal, G., Banerjee, A., Bhaumick, C., Sutradhar, S. and Bandyopadhyay, A. (2024). The Influence of Nd^{3+} Doping on the Structural, Optical, Magnetic, and Dielectric Characteristics of Nanoscale Hexagonal Wurtzite Type ZnO. *Journal of Magnetism and Magnetic Materials*, *591*. https://doi.org/10.1016/j.jmmm.2024.171728.

2 Wang, J., Zhu, R., Gao, Y., Jia, Y. and Cai, G. (2023). Unveiling the Multistep Electrochemical Desorption Mechanism of Cubic NiO Films for Transmissive-to-Black Electrochromic Energy Storage Devices. *Journal of Physical Chemistry Letters*, *14*, 2284–2291. https://doi.org/10.1021/acs.jpclett.3c00050.

3 Das, A., Zajac, M., Huang, W.-H., Chen, C.-L., Kandasami, A., Delaunois, F., Noirfalise, X. and Bittencourt, C. (2024). Evolution of Structural Phase Transition from Hexagonal Wurtzite ZnO to Cubic Rocksalt NiO in Ni Doped ZnO Thin Films and Their Electronic Structures. *Physica Scripta*, *99*. https://doi.org/10.1088/1402-4896/ad16b1.

4 Sun, X.W., Liu, Z.J., Chen, Q.F., Chu, Y.D. and Wang, C.W. (2006). Thermal Expansivity and Bulk Modulus of ZnO with NaCl-Type Cubic Structure at High Pressures and Temperatures. *Physics Letters, Section A: General, Atomic and Solid State Physics*, *360*, 362–366. https://doi.org/10.1016/j.physleta.2006.08.045.

5 Lin, L., Liu, T., Miao, B. and Zeng, W. (2013). Hydrothermal Fabrication of Uniform Hexagonal NiO Nanosheets: Structure, Growth and Response. *Materials Letters*, *102-103*, 43–46. https://doi.org/10.1016/j.matlet.2013.03.103.

6 Xu, C., Wei, P., Wei, Z. and Guo, X. (2024). Shear Horizontal Wave in a P-Type Si Substrate Covered with a Piezoelectric Semiconductor n-Type ZnO Layer with Consideration of PN Heterojunction Effects. *Acta Mechanica*, *235*, 735–750. https://doi.org/10.1007/s00707-023-03771-4.

7 Tsay, C.Y., Chen, Y.C., Tsai, H.M. and Lu, F.H. (2023). Photoresponse of Solution-Processed Transparent Heterojunction Ultraviolet Photodetectors Composed of n-Type ZTO and p-Type NiO-Based Semiconductor Thin Films. *Materials Chemistry and Physics*, *295*. https://doi.org/10.1016/j.matchemphys.2022.127143.

8 Chandak, V.S., Kumbhar, M.B. and Kulal, P.M. (2024). Highly Sensitive and Selective Acetone Gas Sensor-Based La-Doped ZnO Nanostructured Thin Film. *Materials Letters*, 357. https://doi.org/10.1016/j.matlet.2023.135747.

9 Thomas, A., Thirumalaisamy, L., Madanagurusamy, S. and Sivaperuman, K. (2024). Switching the Selectivity of ZnO Thin Films for Ultra-Sensitive Acetaldehyde Gas Sensors through Co Doping. *Sensors and Actuators B: Chemical*, 401. https://doi.org/10.1016/j.snb.2023.135043.

10 Nagarjuna, Y. and Hsiao, Y.J. (2024). TeO_2 Doped ZnO Nanostructure for the Enhanced NO_2 Gas Sensing on MEMS Sensor Device. *Sensors and Actuators B: Chemical*, 401. https://doi.org/10.1016/j.snb.2023.134891.

11 Cuong, N.D., Sinh, V.H., Quang, D.T., Hoa, L.T., Tan, V. Van, Mai, H.D., Jeon, K.J., Phuoc, P.H. and Hieu, N. Van. (2024). 3D Porous P-n α-Fe_2O_3/NiO Heteronanostructure for Ultrasensitive H_2S Gas Sensor. *Current Applied Physics*, 59, 153–164. https://doi.org/10.1016/j.cap.2023.12.019.

12 Shi, C., Yu, L., He, X., Zhang, Y., Liu, J., Li, S., Zhang, C., Cao, L., Nan, N., Du, H. and Yin, M. (2024). Vertically Aligned Mesoporous Ce Doped NiO Nanowalls with Multilevel Gas Channels for High-Performance Acetone Gas Sensors. *Sensors and Actuators B: Chemical*, 401. https://doi.org/10.1016/j.snb.2023.134888.

13 Pai, S.H.S., Mondal, A., Barathy T, R., Ajitha, B., Samuel E, J.J. and Reddy, Y.A.K. (2024). Effect of Calcination Temperature on NiO for Hydrogen Gas Sensor Performance. *International Journal of Hydrogen Energy*, *50*, 928–941. https://doi.org/10.1016/j.ijhydene.2023.07.345.

14 Abdulsattar, M.A., Abduljalil, H.M. and Abed, H.H. (2023). Reaction Mechanisms of Pristine and Cu-Doped ZnO Clusters with Ethanol Using Evans-Polanyi Principle. *Emerging Materials Research*, *12*, 60–67. https://doi.org/10.1680/jemmr.22.00149.

15 Sameer, A.K., Jasim, M.N. and Hussein, M.T. (2023). Concentration Effect on the Vibrational and Electronic Properties of $MgXZn_7$-XO_7 Wurtzoids Nanostructure via DFT. *Digest Journal of Nanomaterials and Biostructures*, *18*, 1187–1195. https://doi.org/10.15251/DJNB.2023.184.1187.

16 Eliche-Quesada, D., Felipe-Sesé, M.A. and Fuentes-Sánchez, M.J. (2021). Biomass Bottom Ash Waste and By-Products of the Acetylene Industry as Raw Materials for Unfired Bricks. *Journal of Building Engineering*, *38*. https://doi.org/10.1016/j.jobe.2021.102191.

17 Abdulsattar, M.A. and Mahmood, T.H. (2023). Enhancement of SnO2 Sensitivity to Acetone by Au Loading: An Application of Evans–Polanyi Principle in Gas Sensing. *Optik*, *275*, 170604. https://doi.org/10.1016/j.ijleo.2023.170604.

18 Abdulsattar, M.A. (2023). $GaxIn_2$-XO_3 Surface Pyramids Interaction with Formaldehyde: Thermodynamic and Sensing Analysis. *Karbala International Journal of Modern Science*, *9*, 8. https://doi.org/10.33640/2405-609X.3324.

19 Ashiq, M., Shehzad, R.A., Iqbal, J. and Ayub, K. (2024). Sensing Applications of Graphitic Carbon Nitride (g-C_3N_4) for Sensing SO_2 and SO_3 — A DFT Study. *Physica B: Condensed Matter*, 676. https://doi.org/10.1016/j.physb.2024.415661.

20 Frisch, M.J., Trucks, G.W., Schlegel, H.B., Scuseria, G.E., Robb, M.A., Cheeseman, J.R., Scalmani, G., Barone, V., Mennucci, B., Petersson, G.A., Nakatsuji, H., Caricato, M., Li, X., Hratchian, H.P., Izmaylov, A.F., Bloino, J., Zheng, G., Sonnenberg, J.L., Hada, M., Ehara, M., Toyota, K., Fukuda, R., Hasegawa, J., Ishida, M., Nakajima, T., Honda, Y., Kitao, O., Nakai, H., Vreven, T., Montgomery, J.A.J., Peralta, J.E., Ogliaro, F., Bearpark, M., Heyd, J.J., Brothers, E., Kudin, K.N., Staroverov, V.N., Kobayashi, R., Normand, J., Raghavachari, K., Rendell, A., Burant, J.C., Iyengar, S.S., Tomasi, J., Cossi, M., Rega, N., Millam, J.M., Klene, M., Knox, J.E., Cross, J.B., Bakken, V., Adamo, C., Jaramillo, J., Gomperts, R., Stratmann, R.E., Yazyev, O., Austin, A.J., Cammi, R., Pomelli, C., Ochterski, J.W., Martin, R.L., Morokuma, K., Zakrzewski, V.G., Voth, G.A., Salvador, P., Dannenberg, J.J., Dapprich, S., Daniels, A.D., Farkas, Ö., Foresman, J.B., Ortiz, J. V., Cioslowski, J. and Fox, D.J. (2013). Gaussian 09, Revision D.01. Gaussian, Inc., Wallingford CT.

21 Abdulsattar, M.A. (2024). Effect of Temperature on the Reaction of Pristine and Au-Doped SnO2 Pyramid Clusters with H2: A Transition State Theory Study. *Passer Journal of Basic and Applied Sciences*, *6*, 192–197. https://doi.org/10.24271/PSR.2024.421994.1412.

22 Hussein, M.T. and Abdullah, B.A. (2022). Study The Effect Of Size Variation And Stability On The Electronic And Spectroscopic Properties Of BN Wurtzoids-Diamantane Nanostructure Via Density Functional Theory. AIP Conference Proceedings. https://doi.org/10.1063/5.0112191.

23 Abdulsattar, M.A., Hussein, M.T. and Kahaly, M.U. (2023). Effect of Reduced Graphene Oxide Hybridization on ZnO Nanoparticles Sensitivity to NO_2 Gas: A DFT Study. *Journal of Ovonic Research*, *19*, 153–163. https://doi.org/10.15251/JOR.2023.192.153.

24 Abdulsattar, M.A. and Al-Bayati, K.H.. (2007). Corrections and Parametrization of Semiempirical Large Unit Cell Method for Covalent Semiconductors. *Physical Review B — Condensed Matter and Materials Physics*, *75*, 245201. https://doi.org/10.1103/PhysRevB.75.245201.

25 Abdulsattar, M.A. (2023). The Reaction of Pristine and Rh-Doped SnO_2 Clusters with Acetone: Application of Evans–Polanyi Principle to Transition State Theory. *Journal of Molecular Modeling*, *29*. https://doi.org/10.1007/s00894-023-05710-5.

26 Zhang, H., Chen, W., Li, Y., Song, Z., Zeng, W., Tang, S., Wang, S. and Zhou, D. (2020). Hierarchical Heterostructures of Nanosheet-Assembled NiO-Modified ZnO Microflowers for High Performance Acetylene Detection. *Ceramics International*, *46*, 3574–3581. https://doi.org/10.1016/j.ceramint.2019.10.075.

27 Lin, Y., Li, C., Wei, W., Li, Y., Wen, S., Sun, D., Chen, Y. and Ruan, S. (2015). A New Type of Acetylene Gas Sensor Based on a Hollow Heterostructure. *RSC Advances*, *5*, 61521–61527. https://doi.org/10.1039/c5ra10327d.

28 Shen, Z., Zhang, X., Ma, X., Chen, Y., Liu, M., Chen, C. and Ruan, S. (2018). Synthesis of Hierarchical 3D Porous ZnO Microspheres Decorated by Ultra-Small Au Nanoparticles and Its Highly Enhanced Acetylene Gas Sensing Ability. *Journal of Alloys and Compounds*, *731*, 1029–1036. https://doi.org/10.1016/j.jallcom.2017.10.156.

29 Iftekhar Uddin, A.S.M., Phan, D.T. and Chung, G.S. (2015). Low Temperature Acetylene Gas Sensor Based on Ag Nanoparticles-Loaded ZnO-Reduced Graphene Oxide Hybrid. *Sensors and Actuators, B: Chemical*, *207*, 362–369. https://doi.org/10.1016/j.snb.2014.10.091.

30 Wang, X., Zhao, M., Liu, F., Jia, J., Li, X. and Cao, L. (2013). C_2H_2 Gas Sensor Based on Ni-Doped ZnO Electrospun Nanofibers. *Ceramics International*, *39*, 2883–2887. https://doi.org/10.1016/j.ceramint.2012.09.062.

31 Qiao, P.Y., Zhang, L.X., Zhu, M.Y., Yin, Y.Y., Zhao, Z.W., Sun, H.N., Dong, J.Y. and Bie, L.J. (2017). Acetylene Sensing Enhancement of Mesoporous ZnO Nanosheets with Morphology and Defect Induced Structural Sensitization. *Sensors and Actuators, B: Chemical*, *250*, 189–197. https://doi.org/10.1016/j.snb.2017.04.158.

32 He, K., Jin, Z., Chu, X., Bi, W., Wang, W., Wang, C. and Liu, S. (2019). Fast Response-Recovery Time toward Acetone by a Sensor Prepared with Pd Doped WO_3 Nanosheets. *RSC Advances*, *9*, 28439–28450. https://doi.org/10.1039/c9ra04429a.

33 Goh, J.H., Tan, K.W., Liow, J.E., Khiew, P.S., Chiu, W.S. and Haw, C.Y. (2024). Modulating Oxygen Vacancy of ZnO for Visible-Light Driven Photocatalytic H_2 Evolution via Facile Gas Treatment Approach. *Materials Science in Semiconductor Processing*, *178*. https://doi.org/10.1016/j.mssp.2024.108445.

34 Hosny, N.M. (2011) Synthesis, Characterization and Optical Band Gap of NiO Nanoparticles Derived from Anthranilic Acid Precursors via a Thermal Decomposition Route. *Polyhedron*, *30*, 470–476. https://doi.org/10.1016/j.poly.2010.11.020.